Chemistry Europe
European Chemical Societies Publishing

WILEY VCH

Excellence in Chemistry Research

Announcing our new flagship journal

- Gold Open Access
- Publishing charges waived
- Preprints welcome
- Edited by active scientists

Meet the Editors of *ChemistryEurope*

Luisa De Cola
Università degli Studi di Milano Statale, Italy

Ive Hermans
University of Wisconsin-Madison, USA

Ken Tanaka
Tokyo Institute of Technology, Japan

Chemistry–A European Journal
Research Article
doi.org/10.1002/chem.202300461
Chemistry Europe
European Chemical Societies Publishing
www.chemeurj.org

Special Collection

Stoichiometry-Directed Two-Level Hierarchical Growth of Lanthanide-Based Supramolecular Nanoarchitectures

Daniel Moreno,[a] José Santos,[a, b] Sofia O. Parreiras,[a] Cristina Martín-Fuentes,[a] Koen Lauwaet,[a] José I. Urgel,[a] Rodolfo Miranda,[a, d] Nazario Martín,*[a, b] José M. Gallego,*[c] and David Écija*[a]

Abstract: The design of a well-ordered arrangement of atoms on a solid surface has long been sought due to the envisioned applications in many different fields. On-surface synthesis of metal-organic networks is one of the most promising fabrication techniques. Hierarchical growth, which involves coordinative schemes with weaker interactions, favours the formation of extended areas with the desired complex structure. However, the control of such hierarchical growth is in its infancy, particularly for lanthanide-based architectures. Here the hierarchical growth of a Dy-based supramolecular nanoarchitecture on Au(111) is described. Such an assembly is based on a first hierarchical level of metallo-supramolecular motifs, which in a second level of hierarchy self-assemble through directional hydrogen bonds, giving rise to a periodic two-dimensional supramolecular porous network. Notably, the size of the metal-organic based tecton of the first level of hierarchy can be tailored by modifying the metal-ligand stoichiometric ratio.

Introduction

The synthesis of metal-organic frameworks (MOFs) is already one of the most active fields of research in materials science due to envisioned applications in many different technological and industrial fields.[1,2] MOFs are reticular materials based on metal nodes (or metal clusters) coordinated with organic linkers. The almost endless number of possible metal-organic combinations gives rise to a plethora of coordinative topologies, in terms of crystalline structure, dimensionality, pore shape and size, etc. The recent incorporation of rare-earth elements,[3] motivated by the additional properties that they can provide (magnetism, photoluminescence),[4,5] has also increased the number of available geometries due to their large ionic radii and nature of coordinative interactions, which allow higher coordination numbers.

More recently, the subfields of quasi- (coordination nanosheets)[6] and true (single layer) two-dimensional (2D) MOFs,[7–9] including also lanthanide elements,[10] have experienced a rapid growth due to the additional advantages they offer in terms of ultra-thin thickness and high surface area. In addition, on-surface synthesis has allowed the fabrication of nanoarchitectures not attainable through solution chemistry methods.[11] But even in two dimensions, the large number of distinct interactions involved (molecule-molecule, molecule-metal, metal-metal, for a system of two components, or more if the substrate is to be included), gives rise to a large variety of self-assembly geometries,[9] including complex ones such Archimedean tilings,[12–14] quasycristals,[15] chiral structures,[16] or even hierarchical nanoarchitectures.[17]

In its more general form, "hierarchical self-assembly is the formation of an ordered structure through a set of interactions that decreases in strength".[18] Within the field of 2D MOFs, hierarchical growth refers to those arrangements where, in a first step of hierarchy, small metal-organic coordinated units (tectons) are formed, and in a second step of hierarchy these tectons self-assemble through weaker interactions, usually hydrogen bonds or van der Waals forces.[19] In principle, the number of levels of hierarchy is not limited, but it is quite uncommon to find more than two.[19] Notably the coordinated units are usually small discrete motifs,[16,17,20–23] but they can also be long 1D chains.[24]

In this paper we describe, to the best of our knowledge, a new strategy for hierarchical growth, where the size of the discrete coordinative motifs (tectons) depends on the metal:

[a] Dr. D. Moreno, Dr. J. Santos, Dr. S. O. Parreiras, Dr. C. Martín-Fuentes, Dr. K. Lauwaet, Dr. J. I. Urgel, Prof. Dr. R. Miranda, Prof. Dr. N. Martín, Prof. Dr. D. Écija
IMDEA Nanociencia
C/ Faraday 9, Ciudad Universitaria de Cantoblanco, 28049 Madrid (Spain)
E-mail: nazmar@quim.ucm
david.ecija@imdea.org

[b] Dr. J. Santos, Prof. Dr. N. Martín
Departamento de Química Orgánica
Facultad de Ciencias Químicas
Universidad Complutense, 28040 Madrid (Spain)

[c] Prof. Dr. J. M. Gallego
Instituto de Ciencia de Materiales de Madrid (ICMM), CSIC
Cantoblanco, 28049 Madrid (Spain)
E-mail: josemaria.gallego@imdea.org

[d] Prof. Dr. R. Miranda
Departamento de Física de la Materia Condensada and
Condensed Matter Physics Center (IFIMAC)
Universidad Autónoma de Madrid
Cantoblanco, 28049 Madrid (Spain)

Supporting information for this article is available on the WWW under https://doi.org/10.1002/chem.202300461

Special Collection This publication is part of a Special Collection on aromatic chemistry in collaboration with the "19th International Symposium on Novel Aromatic Compounds (ISNA-19)".

molecule stoichiometric ratio. To this aim, we take advantage of the coordination chemistry of lanthanides on surfaces and their great affinity to establish coordinative links.

Although rare-earth elements have only recently been incorporated into the design and synthesis of 2D MOFs on metal surfaces, there is already a large number of reports using ligands equipped with different functional groups, namely: nitrile,[12,15,25,26] carboxylate,[27–30] or pyridyl.[31,32] Additional 2D organo-metallic networks exploiting C–Ln–C bonds (where C and Ln are carbon and a lanthanide element, respectively) have also been reported.[33] However, linker moieties bearing carbonyl groups have not been used yet to establish coordinative interactions with lanthanides on surfaces. BQAT(4H-benzo[9,1]quinolizino[3,4,5,6,7-defg]acridine-4,8,12-trione) is a planar triangulene derivative, with the central carbon (C) atom replaced by a nitrogen (N) atom, and three electron-withdrawing carbonyl groups that reduce the electron density of the aromatic core (Figures 1a, b). BQAT and other *N*-heterotriangulene derivatives have been studied as good candidates for using in optoelectronic devices.[34–39] More recently, BQAT itself has been used as a precursor to obtain aza-triangulene by on-surface synthesis techniques.[40] The formation of self-assembled structures, coordination networks and covalent networks of some *N*-heterotriangulene derivatives on solid surfaces, mainly coinage metal surfaces, has already been studied.[41–48] In the reported cases, however, the coordinating metal atoms were substrate transition metal adatoms, and the carbonyl groups were not involved in the coordination bond with the metal node.

In particular, in this article we describe how the self-assembly of Dy-BQAT networks on Au(111) proceeds in a hierarchical way, with the unique finding that the size of the coordinated first level hierarchical tecton can be tailored by controlling the Dy:BQAT stoichiometric ratio. Upon Dy deposition on a submonolayer coverage of BQAT on Au(111), Dy-BQAT metallo-suplamolecular units, composed of three BQAT molecules coordinated to one Dy atom, are formed. These tectons self-assemble through hydrogen bonds to form a porous network featuring a hexagonal geometry. When increasing the Dy coverage, the overall symmetry of the system remains unchanged, but now the first level hierarchical tectons are composed of six BQAT molecules coordinated to three Dy atoms. Like in the previous case, the rims of such six-membered supramolecule interact with the adjacent ones through hydrogen bonds, giving rise to a hexagonal supramolecular porous network. Thus, it is feasible to tune the size of the tecton by varying the metal to molecule stoichiometry.

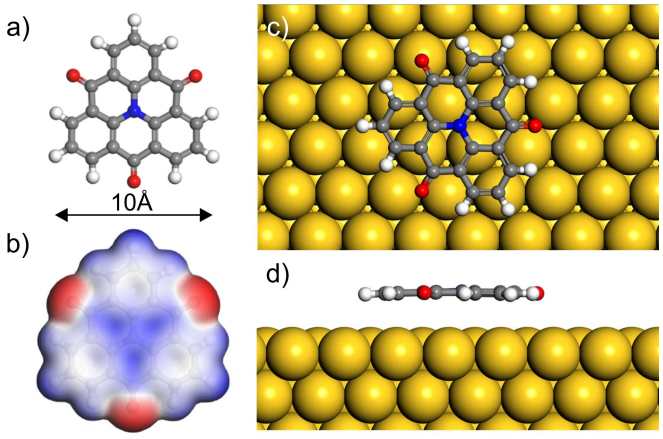

Figure 1. Structural details of BQAT molecule. a) Structure of the BQAT molecule. b) Electronic isosurface (0.02 e-/Å3) colored according to the electrostatic potential. The color scale goes from red (more negative) to blue (more positive). c,d) Top (c) and side (d) views of the DFT optimized structure of an isolated BQAT molecule on Au(111). C, N, O, H and Au atoms are shown in grey, blue, red, white, and yellow, respectively.

Results and Discussion

Figure 2 shows STM images taken after depositing a submonolayer coverage of BQAT on the Au(111) surface, with the substrate held at room temperature, which reveal the formation of two different self-assembled patterns coexisting on the same sample (see Supporting Information, Figure SI1), although each one of them can extend over tens of nanometers (Figures 2a,b). Zoomed-in STM images of the two self-assemblies are shown in Figures 2c,d. The one shown in the left panel of Figure 2 (termed α-phase) is more compact, with all the molecules sharing the same orientation, almost parallel to one of the close-packed directions of the Au(111) surface. The unit cell (yellow line) is hexagonal, with a lattice parameter a = 11.5 (± 0.4) Å, and is compatible with a 4×4 superstructure with respect to the unit cell of the Au(111) surface (Figure SI2a). Each unit cell contains only one BQAT molecule.

The second type of self-assembly (termed β-phase, Figure 2b, d) is a porous one, also with a hexagonal unit cell and a lattice parameter a = 28.3 (±0.4) Å. Each unit cell contains six BQAT molecules and is composed of two triangular sets based on three molecules, with all the molecules in a set sharing the same orientation, also parallel to one of the close-packed directions of the (111) surface. In the following, we will term these sets three-membered supramolecules. The length and orientation of the unit cell are compatible with a commensurate structure that in standard matrix notation can be described as $\begin{pmatrix} 11 & 3 \\ -3 & 8 \end{pmatrix}$ with respect to the crystallographic directions of the Au(111) surface (Figure SI2b).

Figures 2e, f show high-resolution STM images acquired with a carbon monoxide (CO)-functionalized tip,[49] where the internal structure of the molecules can be clearly discerned. DFT optimized models of the self-assemblies for free-standing layers are shown in Figures 2g and the upper half of 2 h. The STM images show that in both phases the molecules are oriented always in the same direction (or rotated ±60°), with their two-fold axis parallel to the high symmetry directions of the gold surface. We have used DFT theoretical calculations to find out the optimal configuration of a BQAT molecule on Au(111). The results are shown in Figures 1c,d. In the minimum energy configuration, the molecule lies almost flat on the

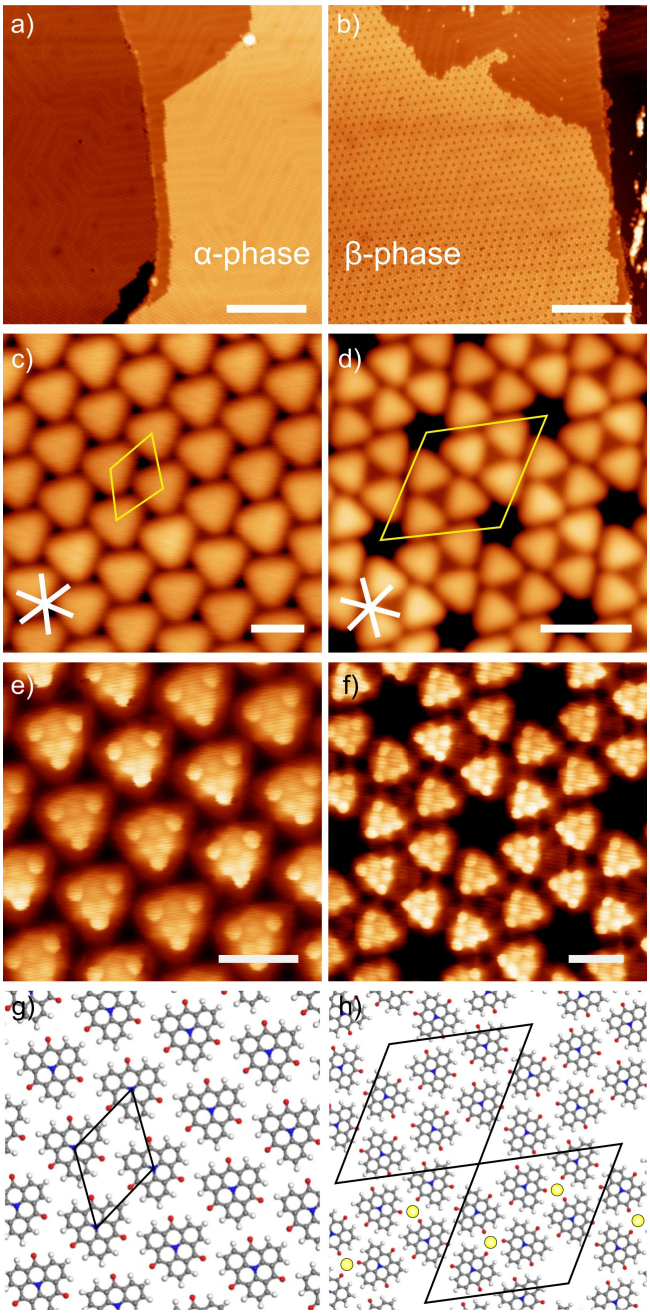

Figure 2. Synthesis of two different BQAT self-assembled phases on Au(111). a, b) STM images showing the existence of two different types of self-assembly, named α (left panel) and β (right panel) phases, after depositing BQAT species on Au(111) at room temperature. c, d) Close-up images of the two phases. The yellow lines indicate their respective unit cells, while the white stars mark the high symmetry direction of the Au(111) surface. e, f) High resolution STM constant current images of both phases taken with a CO functionalized tip. g, h) DFT optimized models of free-standing layers of the two phases. The black lines indicate the unit cells. The yellow dots in (h) highlight the possible existence of Au adatoms. *Scanning parameters: a) $V_b = 0.5$ V; $I_t = 20$ pA; scale bar: 25 nm. b) $V_b = 0.2$ V; $I_t = 300$ pA; scale bar: 25 nm. c) $V_b = 0.05$ V; $I_t = 100$ pA; scale bar: 1 nm. d) $V_b = -1$ V; $I_t = 100$ pA; scale bar: 2 nm. e) $V_b = 0.005$ V; $I_t = 80$ pA; scale bar: 1 nm. f) $V_b = 0.005$ V; $I_t = 70$ pA; scale bar: 1 nm.*

surface, with its 2-fold symmetry axis parallel to the high symmetry directions of the surface, in agreement with the experimental results. The N atom is in a bridge position, and so are two of the O atoms, while the third one is on top. The average height above the last gold layer is 3.4 Å, while the adsorption energy is ~3.16 eV. The charge transfer with the substrate, however, is almost zero (0.07 $|e^-|$).

The STM image displayed in Figure 2c, and the DFT results in Figure 2g, show that in the compact α-phase the molecules are interacting through hydrogen bonds between the oxygen atoms and the terminal hydrogen atoms of adjacent species. The structure of the porous β-phase, however, is more complex (Figures 2d and 2 h). At first sight, the geometrical configuration within a three-membered supramolecule would seem energetically unfavorable, since the partially negative O atoms (see Figure 1b) point directly towards each other. There are two possible explanations for this apparently anomalous configuration: i) *There is no Au atom involved* (Figure 2h, top half): A careful examination of the data reveals that there is a small rotation (~6°) of every molecule around its molecular center (see Figure SI3a). This decreases the electrostatic repulsion between the O atoms and favors the formation of a hydrogen bond between one O atom and one H atom of the neighboring molecule. Actually, DFT calculations of a free-standing layer with a geometry based on the experimental results give a CH–O distance of ~3.3 Å, and a total binding energy for a three-membered supramolecule of ~0.19 eV (Figure SI3b). ii) *The three oxygen atoms are coordinated to a gold atom located at the center of the supramolecule* (Figure 2h, bottom half): This gold atom could be a true gold adatom, or a substrate atom slightly pulled out of the surface by the negatively charged oxygen atom.[43,50,51] However, as shown above, the interaction of the BQAT molecule with the surface is rather weak, so the second explanation seems unlikely. And although most of the images do not show indication of the presence of a gold adatom, as it is often the case in STM or nc-AFM images of metal-organic frameworks,[52–55] STM images taken at rather extreme conditions (Figure SI4) do indeed show a small protuberance (or a dip, depending on the tunneling conditions), demonstrating that there is actually a gold atom located at the center of the supramolecule. The source of the gold adatoms could be the herringbone reconstruction, but this usually results in the lifting of the herringbone reconstruction,[13,56] which is not the case here since the reconstruction is clearly visible underneath the β-phase (Figure SI5). The remaining option is the kinks and steps at the surface, as it has been reported before,[57] since gold atoms are known to diffuse at room temperature on the Au(111) surface.[58,59]

Next, we deposited Dy to inspect the coordination capabilities of BQAT with lanthanides on the Au(111) surface. Figures 3a, b show STM images taken after depositing Dy on a Au(111) surface previously covered by a submonolayer amount of BQAT, with the substrate held at room temperature.

The STM images illustrate that the spatial extent of the α-phase has decreased noticeably (although not visible in Figure 3a, there are still small areas of the α-phase present on the surface, see Figure SI6). On the other hand, most of the surface is dominated by a hexagonal porous supramolecular network (that will be termed $\beta_{Dy}(3)$), very similar to the previous β-phase,

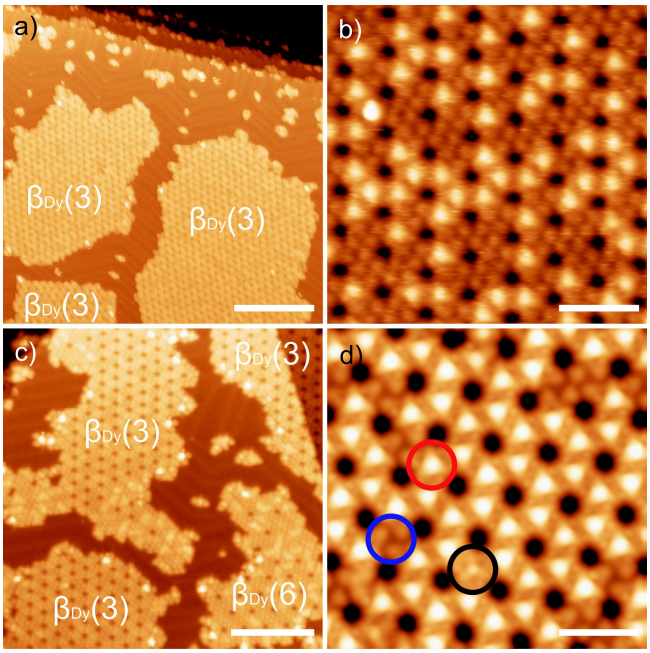

Figure 3. STM images taken after depositing increasing amounts of Dy on a submonolayer coverage of BQAT on Au(111). a,b) 20 s of Dy; c,d) 40 s of Dy. *Scanning parameters: a) $V_b = -0.7$ V; $I_t = 100$ pA; scale bar: 25 nm. b) $V_b = 0.5$ V; $I_t = 100$ pA; scale bar: 4 nm. c) $V_b = 0.5$ V; $I_t = 100$ pA; scale bar: 13 nm. d) $V_b = 0.5$ V; $I_t = 50$ pA; scale bar: 4 nm.*

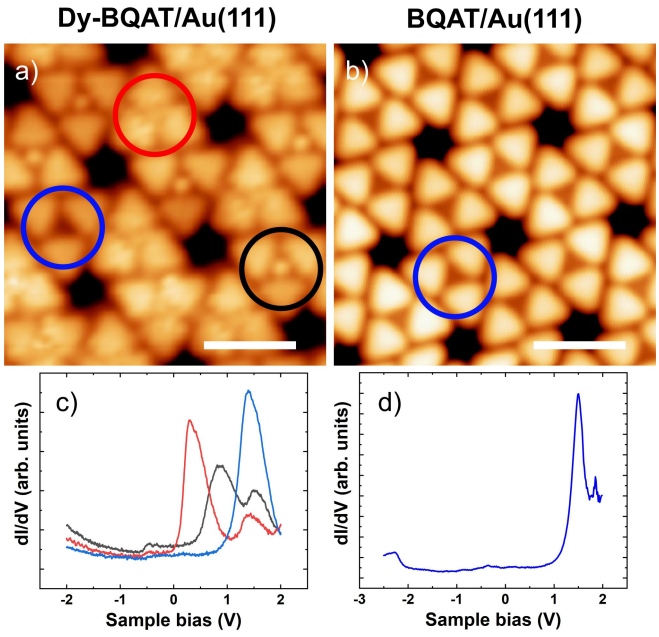

Figure 4. Electronic structure of the dinsctinct nodes. a) STM image of a region of the $\beta_{Dy}(3)$-phase showing the three different types of nodes. (b) STM image of the β-phase (without Dy). c,d) dI/dV spectra taken at the centers of the circles indicated in (a) and (b). *Scanning parameters: a) $V_b = -0.7$ V; $I_t = 0.2$ nA; scale bar: 2 nm; b) $V_b = -1.0$ V; $I_t = 0.1$ nA; scale bar: 2 nm. Open feedback parameters for dI/dV spectra: c) $V_b = 2$ V; $I_t = 500$ pA; $V_{rms} = 20$ mV. d) $V_b = -2.5$ V; $I_t = 130$ pA; $V_{rms} = 20$ mV.*

but with some nodes appearing much brighter at almost any positive voltage (Figure SI7). Since their number increases with Dy deposition time (compare Figures 3b and 3d), we attribute them to Dy atoms located at the center of the supramolecules. A careful inspection (and optimal tip conditions) shows that actually there are three different types of nodes in this $\beta_{Dy}(3)$ phase (Figure 4a). As scanning tunneling spectroscopy shows (Figure 4), type 1 nodes (blue circle) are very similar to those found before Dy deposition, so the two new types (2, black circle, and 3, red circle) must be associated to the presence of Dy atoms. In fact, atom manipulation experiments (Figure SI8) reveal that both types of nodes can transform into each other (by either scanning at high voltages or applying pulse voltages). The highest resolution STM images show type 2 (black) as a definite single round protuberance, so it is most possibly related to the presence of a single Dy atom at the node. There are different possible explanations for the nature of type 3: a different type of Dy configuration (with, for example, a different height above the Au surface), a dimer composed of a Dy atom on top of the gold adatom, or a dimer composed of two Dy atoms, to name a few. However, the ease by which both types can transform into each other make us think that type 2 is just composed of a contaminant adsorbate on top of a Dy atom (since it does not appear in the absence of Dy), which would be able to diffuse over the surface under the influence of the scanning tip or the applied electric field. In any case, both type 2 and type 3 nodes are based on Dy atoms.

Upon further Dy deposition (Figures 3c,d) the α-phase disappears almost completely, while, as mentioned above, the number of Dy nodes in the so-called $\beta_{Dy}(3)$-phase increases considerably. Note that for larger Dy coverages this phase becomes an (almost) Dy-only coordinated $\beta_{Dy}(3)$-phase, with a Dy:BQAT stoichiometric ratio of 1:3 (Figure 3d). This would be a clear example of hierarchical growth: the three-membered supramolecules, which would be based on the coordination to a Dy atom, self-assemble by hydrogen bonds to form the porous lattice.

However, the most noticeably effect of the increment of Dy deposition, and thus the rise of the metal to molecule stoichiometry, is the appearance of a new phase (to be termed $\beta_{Dy}(6)$, Figure 3c and Figure 5). This phase is quite similar to the $\beta_{Dy}(3)$-phase, but in a first level of hierarchy it is based on six-membered supramolecules in which the BQAT species are coordinated to three Dy atoms, as depicted in the model in Figure 5b. In a second level of hierarchical order, the six-membered supramolecules form a hexagonal porous network based on hydrogen bonds. Such a self-assembly was never observed in the absence of Dy, even after annealing the sample, so we can safely assume that in the first level of hierarchical self-assembly all the molecules are coordinated with Dy atoms. Notice that the stoichiometry of this new phase is Dy:BQAT = 1:2. Thus, we can conclude that, in the Dy-BQAT self-assembly, the size of the coordinated supramolecule in the first level of hierarchy depends on the Dy:BQAT stoichiometric ratio. Note that in this new phase there are also two types of nodes, one clearly brighter than the other in Figure 5a, thus resembling the type 2 (black) and 3 (red) nodes found in the $\beta_{Dy}(3)$-phase.

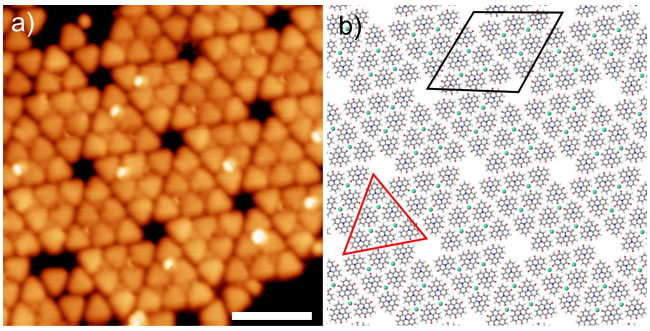

Figure 5. Hierarchical growth of the Dy-BQAT coordination network. a, b) STM images after deposition of Dy on a submonolayer coverage of BQAT on Au(111). *Scanning parameters:* $V_b = 0.05$ *V;* $I_t = 80$ *pA; scale bar: 3 nm.* b) Schematic model of the $\beta_{Dy}(6)$ phase. The black line indicates the unit cell, while the red triangle shows the coordinated supramolecule.

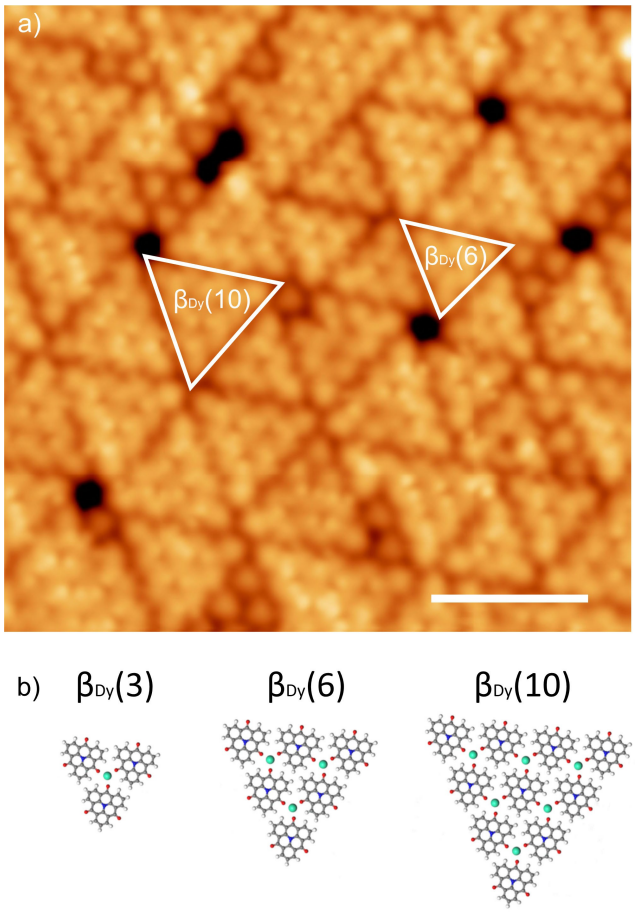

Figure 6. Increment of the size of the coordinative tecton size by annealing Dy-BQAT network to 373 K. a) STM image after annealing. b) Scheme of the different supramolecules that form the first level of hierarchical growth depending on the Dy:BQAT stoichiometric ratio: 1:3, 3:6, and 6:10 for $\beta_{Dy}(3)$, $\beta_{Dy}(6)$, and $\beta_{Dy}(10)$, respectively. *Scanning parameters: (a)* $V_b = 300$ *mV;* $I_t = 100$ *pA; scale bar: 5 nm.*

Importantly, the coordinated unit can be made even larger by annealing the sample. Figures 6a shows an STM image taken after annealing to 373 K. The general structure of the assembly is very similar, but now there is a coexistence of supramolecular units composed of 6 and 10 molecules. Herein, annealing has improved the ordering of the sample by promoting the diffusion of previously uncoordinated Dy atoms. Actually, the STM images (Figure SI9) show that before annealing there are some Dy clusters present on the surface that disappear after annealing. However, apparently in this case there is not enough Dy to build a complete $\beta_{Dy}(10)$ phase based exclusively on 10-membered supramolecules.

Ideally, and disregarding kinetic limitations, for a perfect Dy:BQAT = 1:1 stoichiometry an extended Dy-BQAT fully coordinated network could be expressed. We have tried to create this network by different procedures (increasing the Dy ratio, trying different annealing rates and temperatures), but unfortunately it was impossible to obtain a single continuous layer. Figure SI10 shows the best results obtained after different attempts. As expected, the size of the triangular units increases considerably, but they do not get to form a single-domain coordinated network, still existing molecules with two different orientations. The overall structure of the Dy-BQAT molecular arquitecture somehow resemble those results reported in Ref[60], where trimesic acid molecules self-assembly at room temperature on Au(111) to form also triangular units, with two different orientations, which size increases with molecular coverage. In that case, however, it was possible to form a single-domain close-packed structure just by approaching a full monolayer coverage. The difference with our case is that there are no coordination bonds in there, the molecules being held together by hydrogen bonds only, both between adjacent triangular units, but also within the triangular units. It seems then that it is the strength of the coordination bond what does not allow the detachment of a molecule from a triangular unit to diffuse, rotate and merge an adjacent island with a different orientation. Nevertheless, we have performed DFT calculations for a free-standing layer with such a structure (Figure SI11). The results give a semiconducting layer with a very low band-gap (0.06 eV), where the Dy atoms form a hexagonal lattice and are separated by ~11.1 Å. The Dy atoms are positively charged ($q = 1.5\,|e^-|$), and each one holds a magnetic moment of 4.2 μ_B. In principle, these results should also be, approximately, valid for the larger triangular units. It is also important to note that we could not find a unit cell commensurate with the Au substrate with this lattice parameter and the experimentally found orientation. This could be and additional reason for the impossibility to grow a single-domain compact layer.

Conclusion

In summary, we report here the on-surface synthesis of a Dy-based supramolecular network whose assembly is guided by a two-level hierarchy. Dy and BQAT species first form coordinated supramolecular units based on unprecedented carbonyl-lanthanide interactions. On a second level of hierarchy the metal-organic supramolecules are assembled by hydrogen bonds to form hexagonal porous lattices. Importantly, the size of the coordination units can be augmented by increasing the metal

to molecule stoichiometry. Our study leads the way for the design of complex supramolecular architectures on surfaces, providing new insights into the chemistry of lanthanides on surfaces.

Experimental Section

The scanning tunnelling microscopy (STM) experiments were performed in IMDEA Nanoscience in an ultra-high vacuum (UHV) setup with a base pressure of 1×10^{-10} mbar, hosting a commercial low-temperature STM from Omicron held at cryogenic temperatures (4.3 K, LakeShore). The images have been taken in constant current mode unless otherwise is stated, with a bias voltage applied to the sample, employing electrochemically etched Au tips.

Prior to start the experiments, the Au(111) crystal was prepared by repeated cycles of standard Ar^+ sputtering (1.5 keV, 10 μA, 10 min, SPECS IQE 11/35) and subsequent annealing to 723 K during 10 min.

BQAT linkers were deposited on top of the clean substrate held at room temperature by molecular beam epitaxy from a quartz crucible held at 480 K (Kentax TCE-BSC). To control the deposition, molecular flux was monitored by means of a quartz crystal microbalance (LewVac). To form the metal-organic structures $\beta3$ and $\beta6$, Dy atoms were deposited from previously degassed rods (EFM3Ts evaporator) at a typical flux current of 1.15 nA on top of the crystal held at room temperature and previously covered by less than one monolayer of BQAT species to have enough space for the metal-organic phase to be expressed. Subsequent annealing of this sample at 373 K during 30 min produces an increment of the coordinated unit as stated in the main text.

All the images showed in this manuscript have been analysed and processed with WSxM software.[61]

DFT calculations were carried out using the DMol3 package[62,63] integrated in the Material Studio program of Dassault Systèmes. The electron exchange and correlation energies were treated with the generalized gradient approximation (GGA) of Perdew, Burke, and Ernzerhof.[64] The valence electron functions were expanded to a set of numerical atomic orbitals by a double-numerical basis with polarization functions (DNP), (a polarization d function on all the non-hydrogen atoms and a polarization p function on all the hydrogen atoms). The cutoff radius was set to Rc = 3.7 Å for the free-standing layers and 4.5 Å for the isolated molecule on Au(111). DFT semicore pseudopotentials (DSPP),[65] which include some degree of relativistic effects, were used for Au. The Tkatchenko and Scheffler (TS) scheme[66] for dispersion correction was also included. The convergence criteria were as follows: SCF tolerance, 2.7×10^{-5} eV; maximum displacement, 2.0×10^{-3} Å; maximum force, 2.7×10^{-2} eV/Å; and total energy, 2.7×10^{-5} eV.

For the isolated BQAT molecule on Au(111), the metal surface was simulated by a repeated four layers slab where the two bottom layers were kept frozen, with a lateral 6×6 supercell and a unit cell length in a perpendicular direction of 50 Å, in order to avoid the interaction between adjacent structures. In all cases the Brillouin zone was sampled by $3\times3\times3$ Monkhorst-Pack mesh.[67]

Acknowledgements

This project has received funding from the European Research Council (ERC, grant 766555) and Marie Sklodowska-Curie Actions (MSCA, project 894924) under the European Union's Horizon 2020 research and innovation program, from the EMPIR Programme co-financed by the Participating States and the European and Union's Horizon 2020 Research and Innovation Programme (grant EMPIR 20FUN03 COMET), from Spanish MINECO (PID2019-108532GB-I00 and PID2020-114653RB-I00) and from Comunidad Autónoma de Madrid via 'Programa de Investigación Tecnologías' 2018 (FOTOART-CM S2018/NMT-4367, NANOMAGCOST S2018/NMT-4321) and through project QUIMTRONIC-CM (Y2018/NMT-4783). This study was also supported by MCIN with funding from European Next Generation EU (PRTR-C17.I1, MAD2D-CM-UCM1-MRR and MAD2D-CM-IMDEA Nanociencia projects). NM and JS thank the financial support by the ERC (SyG TOMATTO ERC-2020-951224). IMDEA Nanociencia acknowledges funding from the 'Severo Ochoa' and 'María de Maeztu' Programs for Centers of Excellence in R&D (MINECO, Grants SEV-2016-0686 and CEX2020-001039-S).

Conflict of Interest

The authors declare no conflict of interest.

Data Availability Statement

The data that support the findings of this study are available from the corresponding author upon reasonable request.

Keywords: hierarchical growth · lanthanides · metal-organic networks · on surface synthesis · STM

[1] J. R. Long, O. M. Yaghi, *Chem. Soc. Rev.* **2009**, *38*, 1213–1214.
[2] H. Furukawa, K. E. Cordova, M. O'Keeffe, O. M. Yaghi, *Science* **2013**, *341*, 10.1126/SCIENCE.1230444.
[3] C. A. Black, J. S. Costa, W. T. Fu, C. Massera, O. Roubeau, S. J. Teat, G. Aromí, P. Gamez, J. Reedijk, *Inorg. Chem.* **2009**, *48*, 1062–1068.
[4] A. K. Bar, P. Kalita, M. K. Singh, G. Rajaraman, V. Chandrasekhar, *Coord. Chem. Rev.* **2018**, *367*, 163–216.
[5] Y. Cui, B. Chen, G. Qian, *Coord. Chem. Rev.* **2014**, *273–274*, 76–86.
[6] R. Sakamoto, K. Takada, T. Pal, H. Maeda, T. Kambe, H. Nishihara, *Chem. Commun.* **2017**, *53*, 5781–5801.
[7] J. V. Barth, *Surf. Sci.* **2009**, *603*, 1533–1541.
[8] Y. Fang Geng, P. Li, J. Zhen Li, X. Mei Zhang, Q. Dao Zeng, C. Wang, *Coord. Chem. Rev.* **2017**, *337*, 145–177.
[9] L. Dong, Z. A. Gao, N. Lin, *Prog. Surf. Sci.* **2016**, *91*, 101–135.
[10] D. Écija, J. I. Urgel, A. P. Seitsonen, W. Auwärter, J. V. Barth, *Acc. Chem. Res.* **2018**, *51*, 365–375.
[11] S. Clair, D. G. De Oteyza, *Chem. Rev.* **2019**, *119*, 4717–4776.
[12] D. Écija, J. I. Urgel, A. C. Papageorgiou, S. Joshi, W. Auwärter, A. P. Seitsonen, S. Klyatskaya, M. Ruben, S. Fischer, S. Vijayaraghavan, J. Reichert, J. V. Barth, *Proc. Natl. Acad. Sci. USA* **2013**, *110*, 6678–6681.
[13] Z. Shi, N. Lin, *J. Am. Chem. Soc.* **2009**, *131*, 5376–5377.
[14] Y. Zhang, X. Zhang, Y. Li, S. Zhao, S. Hou, K. Wu, Y. Wang, *J. Am. Chem. Soc.* **2020**, *142*, 17928–17932.
[15] J. I. Urgel, D. Écija, G. Lyu, R. Zhang, C.-A. A. Palma, W. Auwärter, N. Lin, J. V. Barth, *Nat. Chem.* **2016**, *8*, 657–662.
[16] A. Dmitriev, H. Spillmann, M. Lingenfelder, N. Lin, J. V. Barth, K. Kern, *Langmuir* **2004**, *20*, 4799–4801.
[17] M. A. Lingenfelder, H. Spillmann, A. Dmitriev, S. Stepanow, N. Lin, J. V. Barth, K. Kern, *Chem. Eur. J.* **2004**, *10*, 1913–1919.
[18] I. S. Choi, N. Bowden, G. M. Whitesides, G. M. Whitesides, I. S. Choi, N. Bowden, *Angew. Chem. Int. Ed.* **1999**, *38*, 10.1002/(SICI)1521-3773(19991018)38:20.

[19] H. Spillmann, A. Dmitriev, N. Lin, P. Messina, J. V. Barth, K. Kern, *J. Am. Chem. Soc.* **2003**, *125*, 10725–10728.
[20] M.-C. Blüm, M. Pivetta, F. Patthey, W.-D. Schneider, M. Blüm, M. Pivetta, F. Patthey, W. Schneider, W. thank Alessandro de Vita, M. Stengel, *Angew. Chem. Int. Ed.* **2005**, *44*, 5334–5337; *Angew. Chem.* **2005**, *117*, 5468–5471.
[21] Y. Wang, S. Fabris, G. Costantini, K. Kern, *J. Phys. Chem. C* **2010**, *114*, 13020–13025.
[22] S. Fabris, S. Stepanow, N. Lin, P. Gambardella, A. Dmitriev, J. Honolka, S. Baroni, K. Kern, *Nano Lett.* **2011**, *11*, 5414–5420.
[23] N. Abdurakhmanova, A. Floris, T. C. Tseng, A. Comisso, S. Stepanow, A. De Vita, K. Kern, *Nat. Commun.* **2012**, *3*, 1–7.
[24] A. Langner, S. L. Tait, N. Lin, R. Chandrasekar, M. Ruben, K. Kern, *Angew. Chem. Int. Ed.* **2008**, *47*, 8835–8838; *Angew. Chem.* **2008**, *120*, 8967–8970.
[25] J. I. Urgel, D. Ecija, W. Auwärter, D. Stassen, D. Bonifazi, J. V. Barth, *Angew. Chem.* **2015**, *127*, 6261–6265; *Angew. Chem. Int. Ed.* **2015**, *54*, 6163–6167.
[26] D. Moreno, B. Cirera, S. O. Parreiras, J. I. Urgel, N. Giménez-Agulló, K. Lauwaet, J. M. Gallego, J. R. Galán-Mascarós, J. I. Martínez, P. Ballester, R. Miranda, D. Écija, *Chem. Commun.* **2021**, *57*, 1380–1383.
[27] J. I. Urgel, B. Cirera, Y. Wang, W. Auwärter, R. Otero, J. M. Gallego, M. Alcamí, S. Klyatskaya, M. Ruben, F. Martín, R. Miranda, D. Ecija, J. V. Barth, *Small* **2015**, *11*, 6358–6364.
[28] B. Cirera, L. Đorđević, R. Otero, J. M. Gallego, D. Bonifazi, R. Miranda, D. Ecija, L. Dorević, R. Otero, J. M. Gallego, D. Bonifazi, R. Miranda, D. Ecija, *Chem. Commun.* **2016**, *52*, 11227–11230.
[29] M. Uphoff, G. S. Michelitsch, R. Hellwig, K. Reuter, H. Brune, F. Klappenberger, J. V. Barth, *ACS Nano* **2018**, *12*, 11552–11560.
[30] S. O. Parreiras, D. Moreno, B. Cirera, M. A. Valbuena, J. I. Urgel, M. Paradinas, M. Panighel, F. Ajejas, M. A. Niño, J. M. Gallego, M. Valvidares, P. Gargiani, W. Kuch, J. I. Martínez, A. Mugarza, J. Camarero, R. Miranda, P. Perna, D. Écija, *Small* **2021**, *17*, 2102753.
[31] G. Lyu, Q. Zhang, J. I. Urgel, G. Kuang, W. Auwärter, D. Ecija, J. V. Barth, N. Lin, *Chem. Commun.* **2016**, *52*, 1618–1621.
[32] J. Liu, J. Li, Z. Xu, X. Zhou, Q. Xue, T. Wu, M. Zhong, R. Li, R. Sun, Z. Shen, H. Tang, S. Gao, B. Wang, S. Hou, Y. Wang, *Nat. Commun.* **2021**, *12*, 1–10.
[33] B. Cirera, J. Björk, R. Otero, J. M. Gallego, R. Miranda, D. Ecija, *J. Phys. Chem. C* **2017**, *121*, 8033–8041.
[34] H. Zhang, S. Wang, Y. Li, B. Zhang, C. Du, X. Wan, Y. Chen, *Tetrahedron* **2009**, *65*, 4455–4463.
[35] Z. Fang, V. Chellappan, R. D. Webster, L. Ke, T. Zhang, B. Liu, Y. H. Lai, *J. Mater. Chem.* **2012**, *22*, 15397–15404.
[36] Y. Tsuchiya, Y. Ishikawa, S.-H. Lee, X.-K. Chen, J.-L. Brédas, H. Nakanotani, C. Adachi, *Adv. Opt. Mater.* **2021**, *9*, 2002174.
[37] M. Hirai, N. Tanaka, M. Sakai, S. Yamaguchi, *Chem. Rev.* **2019**, *119*, 8291–8331.
[38] T. A. Schaub, K. Padberg, M. Kivala, *J. Phys. Org. Chem.* **2020**, *33*, e4022.
[39] N. J. van der Heijden, P. Hapala, J. A. Rombouts, J. van der Lit, D. Smith, P. Mutombo, M. Švec, P. Jelinek, I. Swart, *ACS Nano* **2016**, *10*, 8517–8525.
[40] T. Wang, A. Berdonces-Layunta, N. Friedrich, M. Vilas-Varela, J. P. Calupitan, J. I. Pascual, D. Peña, D. Casanova, M. Corso, D. G. de Oteyza, *J. Am. Chem. Soc.* **2022**, jacs.1c12618.
[41] M. Bieri, S. Blankenburg, M. Kivala, C. A. Pignedoli, P. Ruffieux, K. Müllen, R. Fasel, *Chem. Commun.* **2011**, *47*, 10239–10241.
[42] F. Schlütter, F. Rossel, M. Kivala, V. Enkelmann, J. P. Gisselbrecht, P. Ruffieux, R. Fasel, K. Müllen, *J. Am. Chem. Soc.* **2013**, *135*, 4550–4557.
[43] S. Gottardi, K. Müller, J. Carlos Moreno-López, H. Yildirim, U. Meinhardt, M. Kivala, A. Kara, M. Stöhr, S. Gottardi, K. Müller, J. C. Moreno-López, M. Stöhr, U. Meinhardt, M. Kivala, H. Yildirim, A. Kara, *Adv. Mater. Interfaces* **2014**, *1*, 1300025.
[44] C. Steiner, B. D. Gliemann, U. Meinhardt, M. Gurrath, B. Meyer, M. Kivala, S. Maier, *J. Phys. Chem. C* **2015**, *119*, 25945–25955.
[45] K. Müller, J. C. Moreno-López, S. Gottardi, U. Meinhardt, H. Yildirim, A. Kara, M. Kivala, M. Stöhr, *Chem. Eur. J.* **2016**, *22*, 581–589.
[46] U. Meinhardt, F. Lodermeyer, T. A. Schaub, A. Kunzmann, P. O. Dral, A. C. Sale, F. Hampel, D. M. Guldi, R. D. Costa, M. Kivala, *RSC Adv.* **2016**, *6*, 67372–67377.
[47] C. Steiner, J. Gebhardt, M. Ammon, Z. Yang, A. Heidenreich, N. Hammer, A. Görling, M. Kivala, S. Maier, *Nat. Commun.* **2017**, *8*, 10.1038/NCOMMS14765.
[48] C. Steiner, Z. Yang, B. D. Gliemann, U. Meinhardt, M. Gurrath, M. Ammon, B. Meyer, M. Kivala, S. Maier, *Chem. Commun.* **2018**, *54*, 11554–11557.
[49] D. Velic, E. Knoesel, A. Hotzel, M. Wolf, G. Ertl, *Phys. Rev. Lett.* **1998**, *80*, 2004.
[50] T. C. Tseng, C. Urban, Y. Wang, R. Otero, S. L. Tait, M. Alcamí, D. Écija, M. Trelka, J. M. Gallego, N. Lin, M. Konuma, U. Starke, A. Nefedov, A. Langner, C. Wöll, M. Á. Herranz, F. Martín, N. Martín, K. Kern, R. Miranda, *Nat. Chem.* **2010**, *2*, 374–379.
[51] D. Wegner, R. Yamachika, X. Zhang, Y. Wang, M. F. Crommie, N. Lorente, *Nano Lett.* **2013**, *13*, 2346–2350.
[52] A. Kumar, K. Banerjee, A. S. Foster, P. Liljeroth, *Nano Lett.* **2018**, *18*, 5596–5602.
[53] I. Piquero-Zulaica, Z. M. Abd El-Fattah, O. Popova, S. Kawai, S. Nowakowska, M. Matena, M. Enache, M. Stöhr, A. Tejeda, A. Taleb, E. Meyer, J. E. Ortega, L. H. Gade, T. A. Jung, J. Lobo-Checa, *New J. Phys.* **2019**, *21*, 10.1088/1367-2630/ab150e.
[54] R. Adhikari, G. Siglreithmaier, M. Gurrath, M. Meusel, J. Kuliga, M. Lepper, H. Hölzel, N. Jux, B. Meyer, H. P. Steinrück, H. Marbach, *Chem. Eur. J.* **2020**, *26*, 13408–13418.
[55] X. Liu, A. Matej, T. Kratky, J. I. Mendieta-Moreno, S. Günther, P. Mutombo, S. Decurtins, U. Aschauer, J. Repp, P. Jelinek, S. X. Liu, L. L. Patera, *Angew. Chem. Int. Ed.* **2022**, *61*, 10.1002/anie.202112798.
[56] M. N. Faraggi, N. Jiang, N. Gonzalez-Lakunza, A. Langner, S. Stepanow, K. Kern, A. Arnau, *J. Phys. Chem. C* **2012**, *116*, 24558–24565.
[57] T. A. Pham, F. Song, M. N. Alberti, M. T. Nguyen, N. Trapp, C. Thilgen, F. Diederich, M. Stöhr, *Chem. Commun.* **2015**, *51*, 14473–14476.
[58] R. C. Jaklevic, L. Elie, *Phys. Rev. Lett.* **1988**, *60*, 120–123.
[59] Y. Pan, B. Yang, C. Hulot, S. Blechert, N. Nilius, H. J. Freund, *Phys. Chem. Chem. Phys.* **2012**, *14*, 10987–10993.
[60] Y. Ye, W. Sun, Y. Wang, X. Shao, X. Xu, F. Cheng, J. Li, K. Wu, *J. Phys. Chem. C* **2007**, *111*, 10138–10141.
[61] I. Horcas, *Rev. Sci. Instrum.* **2007**, *78*, 013705.
[62] B. Delley, *J. Chem. Phys.* **1998**, *92*, 508.
[63] B. Delley, *J. Chem. Phys.* **2000**, *113*, 7756.
[64] J. P. Perdew, K. Burke, M. Ernzerhof, *Phys. Rev. Lett.* **1996**, *77*, 3865–3868.
[65] B. Delley, *Phys. Rev. B* **2002**, *66*, 155125.
[66] A. Tkatchenko, M. Scheffler, *Phys. Rev. Lett.* **2009**, *102*, 073005.
[67] H. J. Monkhorst, J. D. Pack, *Phys. Rev. B* **1976**, *13*, 5188–5192.

Manuscript received: February 13, 2023
Accepted manuscript online: March 2, 2023
Version of record online: April 14, 2023